The Astrophysical Journal, 671:628–636, 2007 December 10

ISM STUDIES OF GRB 030329 WITH HIGH-RESOLUTION SPECTROSCOPY[1]

Christina C. Thöne
Max-Planck-Institut für Extraterrestrische Physik, Giessenbachstrasse, 85748 Garching, Germany; and Dark Cosmology Centre, Niels Bohr Institut, Juliane Maries Vej 30, 2100 København Ø, Denmark

Jochen Greiner and Sandra Savaglio
Max-Planck-Institut für Extraterrestrische Physik, Giessenbachstrasse, 85748 Garching, Germany

and

Emmanuël Jehin
European Southern Observatory, Alonso de Cordova 3107, Vitacura, Santiago 19, Chile
Received 2006 November 24; accepted 2007 August 17

ABSTRACT

We present early Very Large Telescope UV-Visual Echelle Spectrograph (VLT UVES) high-resolution spectra of the afterglow of GRB 030329 at redshift $z = 0.16867 \pm 0.00001$. In contrast to other spectra from this burst, both emission and absorption lines were detected. None of them showed any temporal evolution. From the emission lines, we determine the properties of the host galaxy, which has a star formation rate (SFR) of 0.198 $M_\odot$ yr^{-1} and a low metallicity of 0.17 $Z_\odot$. Given the low total stellar host mass $\log M_\star = 7.75 \pm 0.15$ $M_\odot$ and an absolute luminosity $m_B = -16.29$, we derive specific SFRs (SSFR) of $\log \mathrm{SFR} = -8.5$ yr^{-1} and $\mathrm{SFR} = 15.1\, M_\odot\ \mathrm{yr}^{-1}\, L_\star^{-1}$. This fits well into the picture of GRB hosts as being low-mass, low-metallicity, actively star-forming galaxies. The Mg II and Mg I absorption lines from the host show multiple narrow (Doppler width $b = 5$–12 km s^{-1}) components spanning a range of $v \sim 230$ km s^{-1}, mainly blueshifted compared to the redshift from the emission lines. These components are likely probing outflowing material of the host galaxy, which could arise from former galactic superwinds, driven by supernovae from star-forming regions. Similar features have been observed in QSO spectra. The outflowing material has high column densities of $\log N_{\mathrm{Mg\,II}} = 13.99 \pm 0.04$ cm^{-2} and $\log N_{\mathrm{Mg\,I}} = 12.39 \pm 0.04$ cm^{-2} and the nonvariability of the column densities implies a distance of at least 560 pc from the burst, further supporting an outflow scenario.

Subject heading: gamma rays: bursts — quasars: absorption lines

1. INTRODUCTION

Gamma-ray bursts (GRBs) have proven to be one of the lighthouses in the distant universe, since the determination of their cosmological origin in 1997 (van Paradijs et al. 1997; Metzger et al. 1997). Their afterglow spectra, ranging from X-ray to radio, follow a power-law decay and do not seem to show intrinsic lines from the burst itself, although there are some claims of X-ray line detections from the prompt emission (e.g., Butler et al. 2005 and references therein). This makes them well suited as a powerful light source to study the burst environment in the host galaxy and the medium in the line of sight by using absorption lines. In addition, emission lines from the host might be seen on top of the afterglow spectrum and provide important information about the type of galaxy in which GRBs occur. As these galaxies are usually very faint and difficult to detect, GRBs offer a unique possibility to find and study these galaxies in detail.

One of the few other possibilities to study these faint, distant galaxies is through QSO observations (Williams et al. 2005 and references therein). Their spectra often show intervening absorption systems from foreground damped Lyα systems (DLAs) or metal absorption lines such as Mg II (Churchill et al. 2005) associated with galaxies or halos of galaxies. Mg II absorbers are the best studied sample to date, as Mg II is the reddest of the strong metal absorption lines in the interstellar medium (ISM), but C IV, which very likely probes a different region of the ISM, has also been studied for many years. Recently, highly excited lines like O VI have also been discovered in such absorption systems (e.g., Churchill et al. 2000; Tripp & Bowen 2005). With high-resolution spectra, the stronger absorption lines of these QSO absorbers usually have been found to consist of several components spanning velocities up to 300 km s^{-1} (Churchill et al. 2003, 2005). These different components are assumed to originate in different clouds in the absorbing system and are therefore able to give a picture of the ISM structure in these galaxies.

For an increasing fraction of GRBs, spectra of the afterglow can be obtained, especially since the *Swift* satellite (Gehrels et al. 2004) started operating in 2004 December. Depending on the redshift and the wavelength range of the instrument, these spectra may contain emission lines from H II regions in the host galaxy or absorption lines from material inside the host galaxy and/or the intergalactic medium. Emission-line analysis from the host galaxy can be easily performed with low-resolution spectroscopy from the afterglow containing emission lines from the galaxy, or with later observations targeting the galaxy itself. These analyses reveal that the hosts of long GRBs are usually young, irregular, low-mass, low-metallicity, star-forming galaxies (Christensen et al. 2004). To study the ISM structure in the host galaxy through absorption lines, however, higher resolution is needed, which is only available for a few bursts so far, namely GRB 020813 (Fiore et al. 2005), GRB 021004 (Fiore et al. 2005), GRB 030226 (Klose et al. 2004), GRB 030329 (this work), GRB 050730 (Chen et al. 2005; D'Elia et al. 2007), GRB 050820 (Prochaska et al. 2007), GRB 050922C (Piranomonte et al. 2007), GRB 051111 (Penprase et al. 2006; Prochaska et al. 2007), GRB 060218 (Wiersema et al. 2007), GRB 060418

[1] Based on ESO proposal 70.D-0087.

TABLE 1
Log of the Observations

Epoch	Data Set	Date	UT	Days after GRB	Exp. Time (minutes)	R (mag)	Seeing (arcsec)	Air Mass	Wavelength Range (Å)
I	1	2003 Mar 30	03:22:44	0.6556	30	15.27	0.73	1.45	3030–3880 + 4760–6840
			03:55:43	0.6785	30	15.31	1.03	1.49	3730–4990 + 6600–10600
	2	2003 Mar 30	04:29:01	0.7016	30	15.38	0.97	1.59	3030–3880 + 4760–6840
			05:01:53	0.7244	30	15.46	0.75	1.74	3730–4990 + 6600–10600
II	3	2003 Apr 2	00:46:54	3.5474	60	17.24	0.49	1.72	3830–4990 + 6600–10600
			01:51:51	3.5925	60	17.25	0.72	1.49	3030–3880 + 4760–6840

Note.—Dates given are the start of the observations.

(Vreeswijk et al. 2007; Prochaska et al. 2007), and GRB 060607 (Ledoux et al. 2006), most of them detected recently. Absorption lines in these high-resolution spectra usually show several components with a wide range of velocities whose nature is still speculative. Due to the wavelength coverage of the spectra and the position of the absorption and emission lines, there are only very few bursts that contain both. Examples are GRB 990712 (Vreeswijk et al. 2001) and GRB 970508 (Reichart 1998), which had Mg II absorption in addition to the host emission lines. GRB 020813 (Barth et al. 2003) showed weak O II emission in addition to the broad absorption lines containing many velocity components, and GRB 020405 (Masetti et al. 2003) had a weak Ca II absorption line. Only for one burst, GRB 060218 (Wiersema et al. 2007), could high-resolution spectra containing both kind of lines be obtained which show different components in the host absorption and one of the emission lines.

The long GRB 030329 was detected by the *HETE-2* satellite at 11:38:41 UT (Vanderspek et al. 2003) and lasted for $T_{90} = 22.9$ s at high energies. In terms of fluence, it was among the top 1% of all detected GRBs. A bright optical afterglow was detected 1.5 hr after the burst with an R-band magnitude of 12.5 (Peterson & Price 2003). The optical light curve showed a slow decay with a power-law index of $\alpha = -1.2 \pm 0.1$ and several phases of rebrightenings at 1.3, 2.4, 3.1, and 4.9 days (Matheson et al. 2003; Lipkin et al. 2004) after the onset of the burst. From the emission lines of the host in the UVES spectra presented here, a redshift of $z = 0.1685$ was determined (Greiner et al. 2003a).

Due to its brightness and low redshift, a series of low-resolution spectra could be taken over several weeks, which showed for the first time the connection between long-duration GRBs and supernovae (SNe; Hjorth et al. 2003; Matheson et al. 2003; Stanek et al. 2003). Also, for the first time, it was possible to measure the time evolution of the afterglow polarization (Greiner et al. 2003b). Emission-line analysis of the host galaxy was obtained from an extensive low-resolution data set taken with the FORS spectrograph (Hjorth et al. 2003; Sollerman et al. 2005) and spectra from Matheson et al. (2003), who found a star formation rate (SFR) of 0.5 $M_\odot$ yr^{-1} and a moderate metallicity of $12 + \log(\mathrm{O/H}) = 8.5$, but they assumed the upper branch of the metallicity solution. None of them, however, was able to detect any absorption line as the wavelength range of their spectra missed the Mg II lines in the UV.

In this paper, we present high-resolution VLT UVES spectra from the first and the fourth night after the burst. We detect and analyze both emission and absorption lines as shown in § 3. The emission lines are used to derive the redshift, extinction, SFR, and metallicity of the host galaxy in § 4. Section 5 shows the splitting of the host absorption lines into five components and gives a possible interpretation of these components. For the calculations in the paper, we used a $\Omega_\Lambda = 0.7$, $\Omega_m = 0.3$ cosmology, a value of $H_0 = 70$ km s^{-1} for the Hubble constant, and $c = 299,792$ km s^{-1}.

2. DATA SAMPLE

High-resolution spectra of the afterglow of GRB 030329 have been collected with UVES (Dekker et al. 2000), of the ESO VLT, on the nights of 2003 March 30 and April 2 (UT) under good seeing conditions (0.9″–0.7″). Four 30 minute exposures and two 1 hr exposures were secured on the first and fourth night after the burst, respectively, using two different beam splitters (dichroic 1 and 2). Two UVES standard settings were used, the so-called DIC1 (red 346 nm, blue 580 nm), and the DIC2 (red 437 nm, blue 860 nm). This combination allowed us to get on the first observing date two spectra covering the full optical range (303–1060 nm), except for small gaps near 575 and 855 nm, and one similar spectrum on the second observing night. We combined the two spectra of the first night into one epoch in order to improve the signal-to-noise ratio (S/N); the spectra of the fourth night are then called epoch II. The use of a 0.8″ slit width provides a resolving power of $\lambda/\Delta\lambda \sim 55,000$ or 5.5 km s^{-1} (FWHM). The slit was oriented along the parallactic angle in order to minimize losses due to the atmospheric dispersion.

The raw data were reduced using the UVES pipeline (ver. 1.4) implemented in the ESO-MIDAS software package (Ballester et al. 2000). This pipeline reduction includes flat-fielding, bias, and sky subtraction, and a relative wavelength calibration that has an accuracy of ± 0.5 km s^{-1}. The optimum extraction method has been used, which assumes a Gaussian profile for the cross-dispersion flux distribution and is optimized for low S/N spectra. The individual reduced spectra were also corrected for the air mass; however, the atmospheric absorption bands could not be removed because of saturation. No correction for vacuum wavelengths or heliocentric velocities (-16.23 and -17.36 km s^{-1} for the two nights, respectively) was done for the final spectra; this was taken into account later for the redshift determination (see § 4).

We also did an absolute-flux calibration using the master response curves determined by ESO Garching Quality Control[2] (see also Hanuschik 2003). Comparison with photometric data of the afterglow from the literature (Matheson et al. 2003) showed that the continuum of the flux-calibrated spectrum was almost a factor of 2 too low. This discrepancy cannot be explained with bad seeing; it seems, however, to be a common problem in UVES flux calibration. Comparison with FORS spectra taken at the same time suggests that the UVES flux calibration is about a factor of 1.6 too low (Wiersema et al. 2007). We therefore recalibrated

[2] See http://www.eso.org/observing/dfo/quality/UVES/qc/std_qc1.html#response.

TABLE 2
PHOTOMETRY USED FOR THE FLUX CALIBRATION OF THE THREE DATA SETS

Band	λ_{center} (Å)	Mag (0.66 days)	Mag (0.71 days)	Mag (3.57 days)
U.....	3590	15.23 ± 0.02	15.31 ± 0.01	17.25 ± 0.10
B.....	4370	15.92 ± 0.03	15.95 ± 0.01	17.94 ± 0.02
V.....	5445	15.49 ± 0.01	15.69 ± 0.01	17.47 ± 0.01
R.....	7170	15.28 ± 0.05	15.44 ± 0.05	17.13 ± 0.04
I.....	9000	14.81 ± 0.01	14.94 ± 0.01	16.72 ± 0.02

NOTES.—Magnitudes used are interpolations from data presented in Matheson et al. (2003), Lipkin et al. (2004), and A. Kann (2007, private communication).

the spectrum using photometric data from Matheson et al. (2003); Lipkin et al. (2004) obtained at the same time as our spectroscopic observations and fitted them with the extinction curve derived in Kann et al. (2006) for that burst, which already includes the correction for the Galactic extinction of $E(B - V) = 0.025$.

The log of the observations is given in Table 1, and the photometric data used for the calibration are given in Table 2. As an example, the entire reduced spectrum of the second epoch is shown in Figure 1.

3. LINE ANALYSIS

3.1. *Emission Lines*

We detected a range of emission lines from the GRB host galaxy, listed in Table 3. The Balmer series down to Hδ, the forbidden lines [O II] $\lambda\lambda$3727, 3729 and [O III] λ5007, as well as [Ne III] λ3869 could be identified. Hα was also detected although it lies in the middle of the atmospheric A absorption band. Fortunately, it fell between two of the resolved atmospheric absorption lines in the atmospheric A band and is therefore affected very little by absorption (see Fig. 2). Hδ and Hγ could only be detected clearly in the data from the fourth night. Of the two [O III] lines at 4963 and 5007 Å, the 4963 Å line unfortunately falls in the gap of the detector in the red arm, which consists of a mosaic

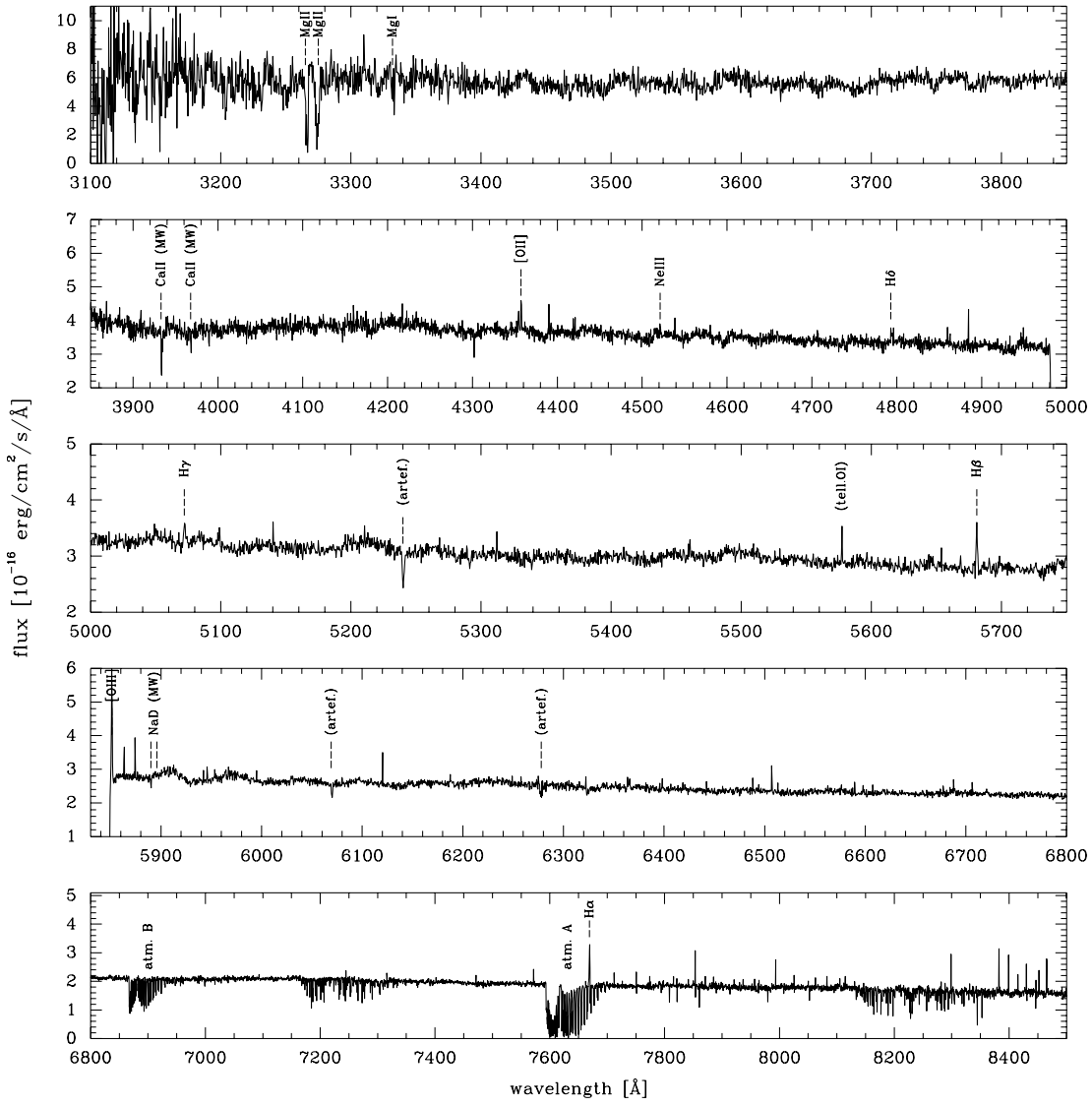

FIG. 1.—Total UVES spectrum of the second epoch, the fourth night after the burst, where the afterglow continuum has faded away enough to result in a good S/N of the host emission lines. For better visualization of the spectral lines in this graph, the spectra have been smoothed and rebinned to 0.4 Å. Ca II and Na D lines are from absorption in the MW; all other absorption and emission lines are from the host galaxy at $z = 0.16867$. The emission features not marked in the middle panel and the second panel from the bottom are due to imperfect atmospheric emission-line removal, as their FWHM is much smaller than from the lines of the host galaxy and they are only visible in the spectra of this epoch. The features at 5238, 6069, and 6975 Å are due to bad pixels or flat-field errors. Note that the scale of the *y*-axis changes for the different panels.

TABLE 3

EMISSION LINE CHARACTERISTICS

Line (1)	Epoch (2)	λ_{rest} (Å) (3)	λ_{obs} (Å) (4)	FWHM (Å) (5)	FWHM (km s^{-1}) (6)	Flux (obs. MW corr.) (10^{-17}ergs cm^{-2} s^{-1} Å^{-1}) (7)	Flux (host A_V corr) (10^{-17}ergs cm^{-2} s^{-1} Å^{-1}) (8)
O II	I	3726.032	(4354)	(0.9)	...	<18.1	<30.6
	II		4354.29	0.91 ± 0.10	64 ± 7	9.89 ± 2.1	16.8 ± 4.2
O II	I	3728.815	4357.67	0.62 ± 0.10	37 ± 7	14.1 ± 2.3	23.9 ± 3.9
	II		4357.43	0.96 ± 0.10	56 ± 7	14.8 ± 2.1	25.1 ± 3.8
Ne III	I	3868.760	4520.80	0.74 ± 0.10	42 ± 6	8.94 ± 3.6	15.0 ± 6.4
	II		4521.27	0.91 ± 0.10	51 ± 6	5.97 ± 1.44	10.0 ± 2.7
Hδ	I	4101.740	(4793)	(0.9)	...	<18.8	<30.8
	II		4793.07	0.83 ± 0.10	45 ± 6	3.35 ± 1.5	5.49 ± 2.8
Hγ	I	4340.470	(5072)	(0.9)	...	<10.8	<17.3
	II		5072.21	0.81 ± 0.10	41 ± 6	6.64 ± 2.0	10.6 ± 3.3
Hβ	I	4861.330	5681.17	0.90 ± 0.10	41 ± 5	13.7 ± 2.0	20.8 ± 4.1
	II		5680.99	1.00 ± 0.10	45 ± 5	13.1 ± 1.6	19.9 ± 2.6
O III	I	5006.843	5850.90	0.77 ± 0.10	33 ± 5	45.7 ± 1.9	68.4 ± 6.2
	II		5851.03	0.76 ± 0.10	33 ± 5	44.7 ± 1.5	66.9 ± 6.1
Hα	I	6562.852	7669.24	1.33 ± 0.10	45 ± 4	32.6 ± 4.1	43.3 ± 5.3
	II		7669.29	1.40 ± 0.10	47 ± 4	32.5 ± 3.0	43.2 ± 4.3
N II	I	6583.450	(7695)	(1.20)	...	<6.20	<8.23
	II		(7695)	(1.20)	...	<1.82	<3.08

NOTES.—Values for the emission lines for the three different data sets, with the numbers indicating the spectra taken in the first and the fourth night after the burst as described in Table 1. The measured wavelengths are in air and are not corrected for heliocentric velocity. FWHM is rest-frame corrected. Fluxes are given as the observed values, corrected for Galactic extinction (col. [7]) and as the values corrected for the host extinction as described in § 4.3 (column [8]). Errors include the errors from the Gaussian fits, the continuum, and the error in the extinction correction, in case of the corrected flux values.

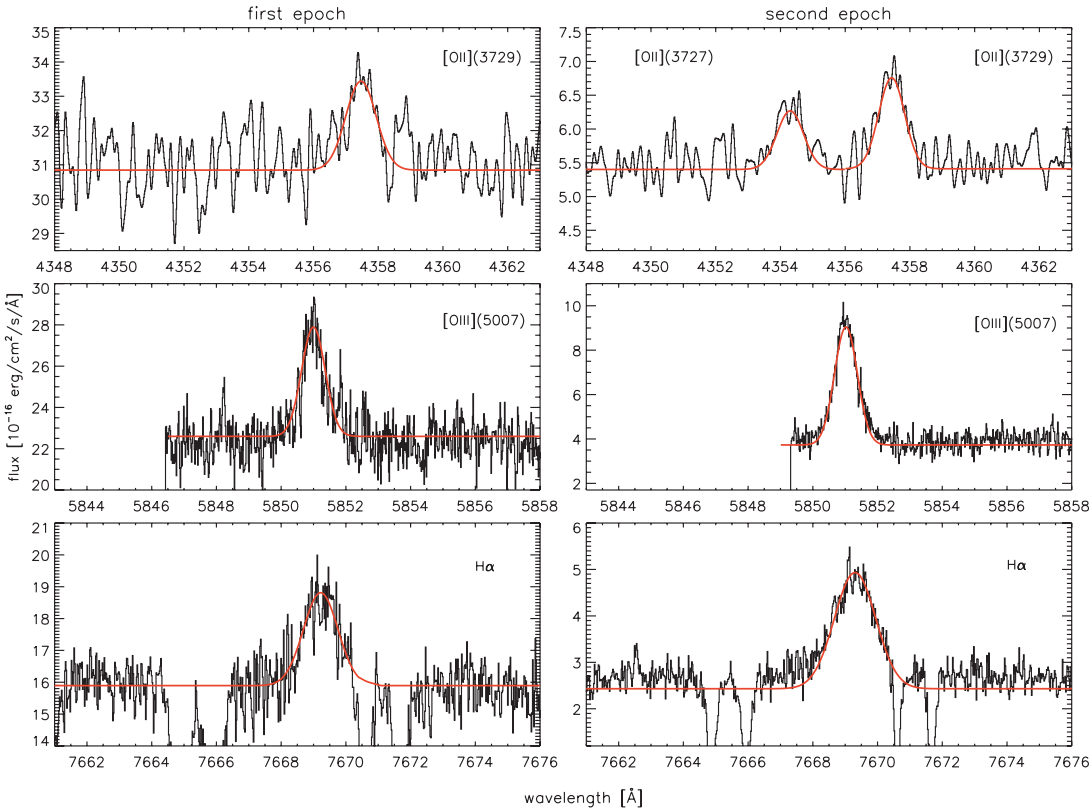

FIG. 2.—Comparison of some selected emission lines at both epochs together with the fitted Gaussians. *Top*: Resolved [O II] $\lambda\lambda$3727, 3729; for better visualization, the spectrum has been smoothed with a boxcar width of 10 pixels. The noise of the continuum in the first epoch is too high to resolve the λ3727 line. *Middle*: [O III] λ5007 near the gap of the spectrum. *Bottom*: Position of the Hα line in between two atmospheric absorption bands.

of two chips. [N II] λ6583 was not detected, but a reliable 2 σ upper limit could be derived because of the high resolution, despite the fact that this region in the spectrum was also affected by atmospheric absorption bands. All upper limits for the flux were derived assuming resolved lines with a FWHM as given in brackets in Table 3. We then used the following formula to calculate the 2 σ upper limits: $f_{\rm limit} = 2[({\rm disp})({\rm npix})\sigma^2]^{1/2}$ where "disp" is the resolution in Å, "npix" is the number of pixels in the FWHM, and σ is the standard deviation of the continuum at the position of the nondetected lines.

The [O II] doublet was well resolved in the spectra of the fourth night (see Fig. 2), which was only possible in three other bursts, GRB 990506 and GRB 000418 (Bloom et al. 2003), as well as GRB 060218 (Wiersema et al. 2007). This is especially interesting because the [O II] $\lambda\lambda$3727/3729 ratio allows the determination of the electron density n_e (Osterbrock 1989). In our spectrum, the ratio of the two lines is 0.53 ± 0.10 for the fourth night's data when the S/N was high enough to resolve the 3727 Å line because the afterglow continuum had faded away. This ratio is consistent with the lower value of 0.66 for $n_e \rightarrow 0$. Similar ratios were found for the hosts of GRB 990506, GRB 000418, and GRB 060218 (see references above) with values of 0.57 ± 0.14, 0.75 ± 0.11, and 0.62 ± 0.05, respectively.

To measure the emission-line fluxes, we fitted the lines with a Gaussian and compared them to measuring the line flux directly, which gave similar results. The flux of the emission lines is constant within the errors for both epochs; the errors are, however, larger for the first epoch due to the higher continuum. We also note that the light curve of the first night showed large variations and even small color changes (Matheson et al. 2003; Lipkin et al. 2004), which might affect the spectrum. For further calculations, we therefore take the emission-line fluxes from the fourth night where all lines were detected and the upper limit for [N II] is smaller due to the lower continuum. After recalibrating the spectra with photometric data, our emission-line fluxes are mostly consistent with the values found by Gorosabel et al. (2005) and Sollerman et al. (2005) in FORS spectra of the host galaxy from 2003 June except for the weak detections of Hδ, Hγ, and [Ne III], where we find higher values; the fluxes noted in these two papers are, however, consistent within our flux errors.

3.2. *Absorption Lines*

Compared to other bursts from which spectra could be obtained, GRB 030329 has a very low redshift. Therefore, most of the metal absorption lines are still far in the UV, below the detection range of UVES.

However, we detect the Mg II $\lambda\lambda$2797, 2803 doublet as clearly resolved, as well as Mg I λ2852, which are all revealed to have several well-resolved velocity components. Voigt profiles (VPs) were fitted to these absorption features using the FIT/LYMAN package (Fontana & Ballester 1995) in MIDAS and the column densities determined for each component (see § 5).

Interstellar Na D $\lambda\lambda$5890, 5896 and Ca II $\lambda\lambda$3933, 3968 from our Galaxy were also detected. The stronger member of the Na D doublet could be resolved into three different clouds, whereas we find only one for the second Na D line, as well as the Ca II doublet. The Na D line is affected by imperfect removal of atmospheric Na D emission, which is worse in the spectra of the second epoch, the equivalent widths (EWs) should therefore be taken with care. The relative line strength of the doublets measured fits well to the expected ratio of about (1 : 1) for both elements. Na and Ca II do not necessarily occur in the same regions in the galaxy, and their wavelength and properties can therefore be different (Welty et al. 1996); however, the lines are too weak in our spectra to derive any conclusion about possible differences in the three absorbing clouds.

TABLE 4
Absorption-Line Characteristics

Line	Epoch	$\lambda_{\rm rest}$ (Å)	$\lambda_{\rm obs}$ (Å)	FWHM (Å)	EW (Å)
Mg II.....	I	2796	3266.1	1.81 ± 0.20	1.34 ± 0.43
	II		3266.7	1.20 ± 0.21	1.15 ± 0.41
Mg II.....	I	2803	3274.6	1.66 ± 0.20	1.01 ± 0.42
	II		3274.8	2.60 ± 0.19	1.76 ± 0.51
Mg I.....	I	2852	3332.8	1.21 ± 0.20	0.22 ± 0.15
	II		3332.9	1.63 ± 0.21	0.34 ± 0.22
Na D.....	I	5890	5889.6	0.21 ± 0.05	0.045 ± 0.023
			5890.0	0.24 ± 0.05	0.034 ± 0.015
			5890.3	...	<0.015
	II		5889.6	0.20 ± 0.05	0.044 ± 0.018
			5890.0	0.10 ± 0.05	0.047 ± 0.018
			5890.3	0.14 ± 0.05	0.029 ± 0.015
	I	5896	5895.6	0.21 ± 0.05	0.018 ± 0.010
			5895.8	...	<0.009
			5896.1	...	<0.009
	II		5895.6	0.11 ± 0.05	0.026 ± 0.024
			5895.8	...	<0.020
			5896.1	...	<0.020
Ca II.....	I	3933	3933.5	0.24 ± 0.04	0.24 ± 0.05
			3934.6	0.29 ± 0.04	0.10 ± 0.05
	II		3933.5	0.51 ± 0.15	0.25 ± 0.16
			3934.5	0.65 ± 0.15	0.11 ± 0.07
	I	3968	3968.3	0.14 ± 0.05	0.09 ± 0.05
	II		3968.3	0.41 ± 0.05	0.12 ± 0.07

Notes.—The Mg lines listed are from the host galaxy; the other lines are from the MW. All values are given in the rest frame. The FWHM of the Mg lines are the widths measured in a spectrum rebinned to 1 Å. Note that the Na D interstellar lines from the second epoch are affected by imperfect sky line removal from telluric Na D emission. Only one component of the Na D λ5896 has a clear detection; for the other components, we only give 1 σ upper limits.

We did not detect any Na D $\lambda\lambda$5890, 5896, Ca II $\lambda\lambda$3933, 3968, or Ti II λ3242 absorption from the host galaxy. The ratio of Ca II to Mg I, which have similar ionization potentials, found in GRB 020813 (Savaglio & Fall 2004) was around 1; in our spectra the limit on this ratio is about 0.1. Ratios found in the Milky Way (MW) can vary between 0.01 and 1 depending on the properties of the ISM (Welty et al. 1999). The properties of the absorption lines are listed in Table 4.

4. RESULTS

4.1. *Redshift*

The redshift of the host galaxy was determined from the [O III] λ5007, Hα, and Hβ emission lines of the first epoch (Greiner et al. 2003a) as $z = 0.1685$. We did a refined analysis using the emission lines [O II] $\lambda\lambda$3726, 3729, [O III] λ5007, Hα, and Hβ, corrected for heliocentric velocities of -16.23 and -17.36 km s^{-1} for epoch I and II, respectively. From this, we derive a value of $z = 0.16867 \pm 0.00001$, consistent with the value found by Matheson et al. (2003) and Sollerman et al. (2005). Note, however, that this is the mean redshift of the GRB host galaxy, not of the GRB itself.

4.2. *Broadening of the Emission Lines*

Low-resolution spectra are usually not able to distinguish between instrumental resolution and intrinsic broadening of the host emission lines due to galaxy rotation and turbulence of the medium. From our high-resolution spectra (FWHM = 5.5 km s^{-1}),

we find that all emission lines in our spectra are clearly broadened compared to the resolution of the instrument. The FWHM of the emission lines lies between 35 and 55 km s^{-1}, rest-frame corrected. This fits well to the fact that the host of GRB 030329 is a dwarf galaxy, which have typical rotational velocities up to 100 km s^{-1}. We might, however, not see the whole rotational velocity spread if the galaxy is not seen edge on.

4.3. *Galactic and Host Extinction*

For the determination of the Galactic extinction, usually sky catalogs such as Schlegel et al. (1998) or Dickey & Lockman (1990) are used. The strength of interstellar lines like Na D, however, allows a different and more accurate determination of the extinction using e.g., the model of Munari & Zwitter (1997) who take the Na D λ5890 line. In our spectra, Galactic Na D as well as Ca II show a triple absorption peak, indicating three clouds in our Galaxy in the line of sight. The Na D line gives an extinction of $E_{B-V} = 0.012 \pm 0.006$, 0.007 ± 0.004, and 0.002 ± 0.001 for the three clouds, respectively, which results in a total extinction of $E_{B-V} = 0.021 \pm 0.014$ or $A_V = 0.065 \pm 0.043$ as $A_V = R_V E_{B-V}$, with $R_V = 3.1$ for a MW extinction law (Cardelli et al. 1989). This is comparable to the extinction determined from the Schlegel sky catalog of $E_{B-V} = 0.025$.

The extinction in the host galaxy can in principle be derived from the Balmer line decrement, the constant flux ratio of the Balmer lines derived from line transition properties, with unextinguished values of $H\alpha/H\beta = 2.76$ and $H\gamma/H\beta = 0.474$ for a temperature of 10,000 K and case B recombination (Osterbrock 1989). From our spectrum we obtain $H\alpha/H\beta = 2.49 \pm 0.2$ and $H\gamma/H\beta = 0.51 \pm 0.15$, which is consistent with no extinction for both epochs. In addition, the Balmer lines can be affected by absorption from an underlying stellar population depending on the age of the galaxy. However, in the UVES spectra, we could not identify any underlying stellar absorption, whereas Gorosabel et al. (2005) derive a relatively high correction, comparable to the value of the fluxes for Hγ and Hδ from their stellar population models. We consider it therefore to be more appropriate to use an extinction value derived from the broadband afterglow as it was done in Kann et al. (2006). They derive a value of $A_V = 0.39 \pm 0.15$, fitting a Small Magellanic Cloud extinction law, which differs, however, very little from the fit with a MW extinction law.

For the correction of the emission-line fluxes of both epochs, we then use $A_V = 0.39 \pm 0.15$ for the host extinction applying a MW extinction law (see Table 3). The photometry used for calibrating the spectrum already includes the correction for the Galactic extinction of $A_V = 0.078$.

4.4. *SFR*

A direct indicator of the current SFR in a galaxy is the flux from nebular emission lines such as Hα that had been ionized by young, massive stars. Using the Hα flux from the third epoch, which is corrected for extinction but not for a possible underlying stellar absorption, we derive a SFR of the host galaxy according to Kennicutt et al. (1998) of SFR $[M_\odot\ \mathrm{yr}^{-1}] = 7.9 \times 10^{-42} 4\pi f_{H\alpha} d_L^2 = 0.198 \pm 0.007\ M_\odot\ \mathrm{yr}^{-1}$, which is consistent with the value in Hjorth et al. (2003) of $\mathrm{SFR}_{H\alpha} = 0.17\ M_\odot\ \mathrm{yr}^{-1}$ from the FORS spectra. Another indicator for the SFR are forbidden lines like [O II] with the drawback of being only indirectly coupled to the ionizing flux of young stars but very sensitive to the ionization state of the ISM. For [O II], the corresponding equation SFR $[M_\odot\ \mathrm{yr}^{-1}] = 1.4 \times 10^{-41} 4\pi f_{[\mathrm{O\,II}]} d_L^2$ gives a value of $0.267 \pm 0.009\ M_\odot\ \mathrm{yr}^{-1}$ taking the sum of the [O II] $\lambda\lambda$3726, 3729 fluxes from the second epoch. As this indicator is less reliable, we therefore adopt here the SFR from Hα.

A SFR of $0.198\ M_\odot\ \mathrm{yr}^{-1}$ is not very high compared to other galaxies at this redshift, but one has to consider the low mass of the host galaxy, as already noted in Sollerman et al. (2005). S. Savaglio et al. (2007, in preparation) derive a low total stellar mass for the host of $M_\star = 10^{7.75 \pm 0.15}\ M_\odot$. This gives a specific SFR (SSFR) per unit mass of $\log \mathrm{SFR}/M = -8.5\ \mathrm{yr}^{-1}$. Furthermore, the host galaxy of GRB 030329 is underluminous with an absolute magnitude of $m_B = -16.29$ (Gorosabel et al. 2005). This can be used to scale the SFR with the luminosity fraction compared to a standard galaxy with $m_{B(\mathrm{abs})} = -21$ to derive the SFR/L (Christensen et al. 2004). For our host, we get a value for the SFR/L of $15.1\ M_\odot\ \mathrm{yr}^{-1}\ L_\star^{-1}$, which is high compared to the average of other host galaxies of $9.7\ M_\odot\ \mathrm{yr}^{-1}\ L_\star^{-1}$ as found by Christensen et al. (2004).

4.5. *Metallicity of the Host*

There are a number of secondary, empirical metallicity calibrators derived from the abundances of nebular emission lines. The most frequently used, being the easiest to measure, is the

$$R_{23} = \frac{f_{[\mathrm{O\,II}]\ \lambda 3727} + f_{[\mathrm{O\,II}]\ \lambda\lambda 4959,\ 5007}}{f_{H\beta}}$$

parameter (Kobulnicky et al. 1999). [O III] λ4959 was not detected due to the gap in the spectrum. There is, however, a fixed ratio between the two [O III] lines, $f_{[\mathrm{O\,III}]\ \lambda 5007} = 3 f_{[\mathrm{O\,III}]\ \lambda 4959}$.

The R_{23} parameter gives two possible solutions, but this degeneracy can be broken using the [N II] λ6583 to Hα ratio (Lilly et al. 2003). As noted in Sollerman et al. (2005) no [N II] was detected in the spectra of GRB 030329, except from the FORS spectrum of May 1 (Hjorth et al. 2003), which seems to be spurious. Due to the high resolution of the UVES spectrum, however, we were able to put a strong 2 σ upper limit of [N II] (see Table 3 and § 3.1) and therefore to derive a ratio of [N II]/Hα from the strongest upper limit at the third epoch of $<0.06 \pm 0.01$, which favors a lower branch solution according to Lilly et al. (2003). We applied both the calibrations for the R_{23} parameter from Kewley & Dopita (2002) used for most GRB host metallicities and the most recent one from Kewley et al. (2007). These parameterizations give then values of $12 + \log(\mathrm{O/H}) = 8.3^{+0.2}_{-0.3}$ and $7.9^{+0.2}_{-0.3}$, respectively, where the errors account for the error in the line fluxes from the second epoch that we use for the calculations. These values correspond to 0.44 and 0.17 $Z_\odot$, assuming $12 + \log(\mathrm{O/H}) = 8.66$ for solar metallicity (Asplund et al. 2004). The low mass of the host galaxy supports a low value for the metallicity.

The R_{23} parameter, however, has turned out to be affected by systematic errors for high and low metallicities (Bresolin et al. 2004). Wiersema et al. (2007) showed that the metallicity of the GRB 060218 host, derived from the oxygen abundances, is $12 + \log(\mathrm{O/H}) = 7.54$, compared to 8.0 from the R_{23} parameter. For a direct calibration from the abundances, however, the electron temperature and density have to be known, which rely on the detection of [O III] λ4363 and the detection of low-error flux measurements of the [O II] $\lambda\lambda$3727, 3729 or [S II] $\lambda\lambda$6716, 6731 doublets, which were not detected for the GRB 030329 host or only with large errors, in the case of [O II].

5. ABSORPTION-LINE KINEMATICS

5.1. *Fitting of the Absorption Systems*

For the absorption lines in the host galaxy, we found five different velocity components for the Mg II doublet which we fitted together, whereas Mg I only shows four because of its

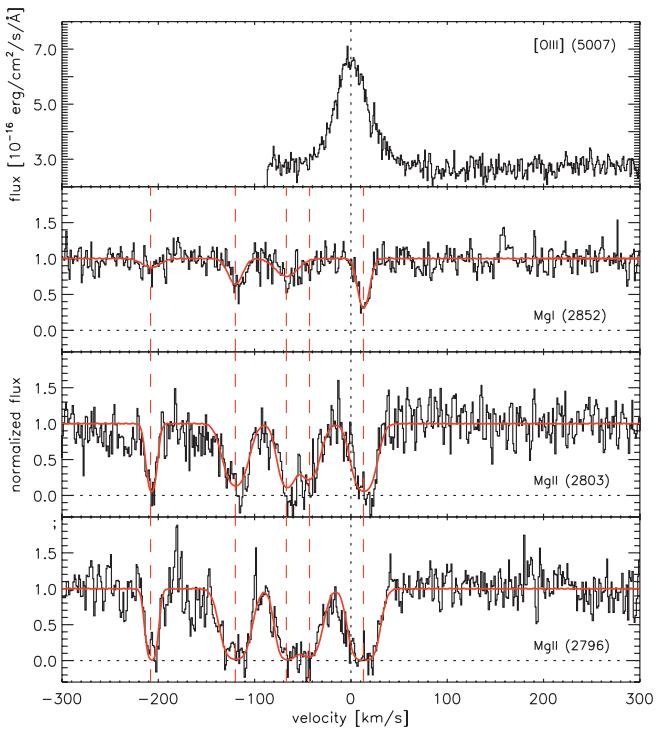

FIG. 3.—Velocity distribution of the five components in the Mg II doublet and four in Mg I and the corresponding fit to the different components with FIT/LYMAN, where the Mg II lines were fitted as doublets. Here, $v = 0$ km s^{-1} corresponds to the redshift determined by the emission lines from the host, where the [O III] line is shown as an example in the top panel. We co-added all three data sets to get better statistics for the fit, as there were no changes in line strength between in the data from the individual epochs.

lower line strength. The components span a velocity range of about 230 km s^{-1} (see Fig. 3) in both Mg II and Mg I. Mg I shows the same velocity differences as the Mg II components, except for the two components at $v = -43$ and -67 km s^{-1}, for which we found only one component in Mg I, so it seems that both arise from the same structure. This does not necessarily have to be the case due to the different ionization stages. The b-parameter of the five components is relatively narrow, with 5–12 km s^{-1}.

No time variability of the absorption lines was seen between the different spectra, and we therefore coadded all three data sets weighted according to their variance in order to improve the S/N. The constant value of the absorption lines rules out an origin in the vicinity of the burst (Perna & Loeb 1998; Prochaska et al. 2006), where one would expect a considerable weakening of the Mg absorption between the first and the fourth night. Furthermore, the Mg II absorption in all components goes down to zero flux, supporting the suggestion that the absorption does not occur at a very short distance from the central source. Otherwise, scattered light could lead to a covering factor smaller than 1 (Savaglio & Fall 2004).

From the absence of Mg I variability in between the two epochs, one can derive a minimum distance to the GRB according to Mirabal et al. (2002; see also Prochaska et al. 2006; Vreeswijk et al. 2007). For the fluence at the position of Mg I, we integrate the flux density in the U band between $t_1 = 0.6$ and $t_2 = 3.5$ days, $F_1 = 1.826 \times 10^{-26}$ ergs s^{-1} cm^{-2} Hz^{-1} and $F_2 = 2.0 \times 10^{-27}$ ergs s^{-1} cm^{-2} Hz^{-1} (data taken from Matheson et al. 2003), assuming a simple power-law evolution between the two epochs. This leads to a number of photons $\phi = 1.27 \times 10^{61}$ at the burst rest frame and at the ionization energy of Mg I of 8.5 eV. We take a very conservative estimate of <25% for the decline of the column densities $N_{\rm I}$ and $N_{\rm II}$ between the two epochs and assume the cross section $\sigma_{\rm ph^{Mg\,I}}$ to be roughly 10^{-18} cm^2, which gives a minimum distance to the GRB of

$$r_{\rm min} = \sqrt{\frac{\phi \sigma_{\rm ph^{Mg\,I}}}{4\pi \ln(N_{\rm I}/N_{\rm II})}} > 560 \text{ pc}.$$

This further supports the suggestion that the absorbing material is not in the vicinity of the burst, as noted above.

The individual components at the different velocity shifts have similar column densities, although comparison of the ratios N(Mg II) to N(Mg I) show that the conditions in the different absorbing structures might vary slightly. The total Mg II column density is $\log N_{\rm Mg\,II} = 13.99 \pm 0.04$ cm^{-2}, which is in the regime of sub-DLAs (Rao & Turnshek 2000). The gas in DLAs has a low ionization and a relatively large column density of $\log N_{\rm Mg\,I} = 12.39 \pm 0.04$ cm^{-2} compared to N(Mg II) as shown in Table 5. Given that portions of the Mg II profiles are beyond the linear part of the curve of growth one may consider the total Mg II column density to be a lower limit.

As the S/N of even the coadded spectrum is quite low, we also performed an apparent optical depth analysis according to Savage & Sembach (1991) in order to check the reliability of our VP fitting. The total column density derived for Mg II is $\log N_{\rm Mg\,II} = 13.9$ cm^{-2}, slightly lower than that derived from VP fitting. This is expected, given that the optical depth analysis is more sensitive to saturation. On the other hand, the Mg I column density is fully consistent with the VP value.

5.2. *Interpretation of the* Mg I *and* II *Velocity Structure*

Mg I and II have been detected in many GRB afterglow spectra (Castro et al. 2003; Fiore et al. 2005; Starling et al. 2005; Penprase et al. 2006; Prochaska et al. 2007). The high-velocity components are usually explained as being connected to the GRB itself like tracing nebula shells from former mass losses of the progenitor star, excited by the GRB (Mirabal et al. 2002) or strong winds that blow material of the star away from the Wolf-Rayet progenitor. The latter scenario was suggested for the high-velocity components in GRB 020813 (Fiore et al. 2005), GRB 021004 (Fiore et al. 2005; Starling et al. 2005), GRB 030226 (Klose et al. 2004), GRB 050505 (Berger et al. 2006), and recently GRB 051111 (Penprase et al. 2006), who found absorption features up to 3000 km s^{-1}. For GRB 021004, however, Chen et al. (2005) argued against the wind scenario due to the detection of low ionization lines in the highest velocity complexes. The velocities measured in GRB 030329, however, are much lower; such winds can therefore not be the explanation for the components seen in our spectra. If those high-velocity features were common for GRBs, they should have also been detected in GRB 030329, in addition to the low-velocity components, but there are no absorption features visible at comparable velocity distance from the main component. Neither were they detected in any other spectra than those of GRBs mentioned above, although the distances are far enough to be resolved in low-resolution spectra as in the case of GRB 021004 (Mirabal et al. 2002). Either the ISM around the burst must be quite dense to produce these clumps, or not all GRB progenitors have high mass loss/winds, or the reason for these components is something completely different.

Since the Mg lines in GRB 030329 have much lower velocity, we have to seek for different explanations. One possibility are supergalactic winds from starburst regions as found in spectra

TABLE 5
Different Components in the Host Absorption Lines

Component (km s^{-1})	Mg II [2796, 2803] b (km s^{-1})	Mg II [2796, 2803] log N (cm^{-2})	Mg I [2852] b (km s^{-1})	Mg I [2852] log N (cm^{-2})	log ($N_{\rm Mg\,I}/N_{\rm Mg\,II}$)
$v_1 = +13$	12.06 ± 0.53	13.45 ± 0.04	6.81 ± 0.85	12.06 ± 0.05	−1.39 ± 0.19
$v_2 = -43$	12.10 ± 0.94	13.17 ± 0.03	...	...	...
$v_3 = -67$	9.77 ± 0.78	13.24 ± 0.05	15.15 ± 5.83	11.75 ± 0.10	−1.49 ± 0.23
$v_4 = -120$	13.09 ± 0.70	13.33 ± 0.04	9.22 ± 1.98	11.74 ± 0.07	−1.59 ± 0.21
$v_5 = -208$	4.82 ± 0.54	13.20 ± 0.15	12.45 ± 4.10	11.35 ± 0.15	−1.85 ± 0.30

Note.—The Mg II doublet was fitted together; therefore, column densities and b-parameters are the same for the two lines of the doublet.

of low-redshift starburst galaxies and clearly visible, e.g., in Hα light from M82. These winds were discovered in X-ray data, as the heated ISM emits X-rays. Heckman et al. (2000) studied the structures of Na D lines from such starburst galaxies. They found blueshifted components relative to the host galaxy up to 600 km s^{-1} with Doppler width of more than 100 km s^{-1}, which seems likely for a hot environment ($T \approx 70{,}000$ K). This, however, rules out the possibility of an active starburst wind for our absorption-line features as the velocities are too low for a wind origin, and in addition the lines are very narrow, so the absorbing atoms cannot be in a hot environment.

In the MW, as well as in other galaxies, so-called "high-velocity clouds" have been found, consisting mainly of H I, but O VI has also been discovered from the same region (Fox et al. 2005). This gave rise to the theory of the galactic fountain where starburst regions blow hot, ionized material out into the halo, which then cools down and eventually falls back again onto the galaxy (Bregman 1980). The Mg absorption lines in our spectra might therefore be caused by some intermediate stages of that process, when the starburst wind has cooled and slowed down. The fact that, except for the two lowest-velocity systems, the velocities are larger than the rotational velocity of the host galaxy as determined from the emission-line width, indicates that they are most likely not just related to large structures in the host galaxy like spiral arms. With the escape velocity typically being less than 50% larger than the mean rotational velocity, half of our velocity systems are likely to be unbound to the gravitational potential of the host galaxy. Further support to an origin outside the galaxy comes from the minimum distance of the Mg I–absorbing material to the GRB of 560 pc for the redmost component. The starburst wind suggestion is therefore an appealing scenario for those structures.

The same process might create Mg II absorbers, which have often been found in the sight lines of QSOs (Ellison et al. 2003) with large EW. Similar structures have also been discovered in Lyman break galaxies (Adelberger et al. 2003) but only for C IV absorption lines. DLAs associated with Mg absorbers show black-bottom saturated Mg velocity components with narrow spreads of about 40–60 km s^{-1}. So-called "doubles" and "classics" have smaller EWs and highly complex features separated by a large Δv (Churchill et al. 2000) with their individual components having Doppler widths comparable to those found in GRB 030329. This might lead to the conclusion that Mg QSO absorbers and GRB absorbers have the same origin but that they are probing different regions of the galaxy. Bond et al. (2001) also suggested that QSO-Mg absorbers could arise in optically thick clouds in the galactic halos, created by material ejection from starburst regions, being the remnants of a former starburst wind.

In contrast to QSO absorbers, which can have lines both redshifted and blueshifted compared to the redshift of the intervening galaxies, there exist in our case only blueshifted lines, except for the first component. This might be a hint to the position of the burst in the galaxy. If these components are really due to some metal-rich clouds in or around the host galaxy, the burst could lie slightly behind the center plane of the galaxy or the starburst cloud that causes the few redshifted components, whereas the rest of the lines come from material flowing away from the burst site.

6. CONCLUSION

In this paper, we have presented two epochs of high-resolution spectra of a typical long-duration GRB at $z = 0.16867$, which had the rare case of containing both emission lines from the host galaxy as well as absorption lines from the surrounding medium of the burst. The host galaxy is a subluminous ($m_B = -16.29$), low mass ($\log M_\star = 7.75 \pm 0.15\, M_\odot$) starburst with a high SFR/L of 15.1 $M_\odot$ yr^{-1} $L_\star^{-1}$ or $\log {\rm SFR}/M = -8.5$ yr^{-1} compared to other galaxies at this redshift. This confirms the values of the SSFR found by Hjorth et al. (2003) and Sollerman et al. (2005) from late FORS spectra of the host galaxy. Furthermore, the high-resolution UVES spectra made it possible to derive a strong upper limit for [N II] and therefore to place the value of the metallicity in the lower branch with $12 + \log({\rm O/H}) = 7.9$, or 0.17 $Z_\odot$.

In absorption, only Mg II and Mg I from the host could be detected. Due to the high resolution, again, however, we were the first to resolve these usually broad absorption lines into eight and five narrow velocity components for Mg I and Mg II, respectively. These components span a relatively small range of velocities up to $v \sim 230$ km s^{-1}, which can usually not be resolved in low-resolution spectra. The majority of these components are, however, outside of the galaxy whose emission lines have only a width of 55 km s^{-1}. Both Mg I and Mg II seem to originate in the same clouds which have a low ionization state as seen from the ratio of the column densities log ($N_{\rm Mg\,I}/N_{\rm Mg\,II}$) of around −1.5. Structures similar in width and velocity distance have been found in QSO Mg absorbers. They could be clouds in the halo of the host galaxy, possibly from material ejected from the inner regions of the galaxy by former starburst-driven superwinds that have already slowed down. An origin far away from the burst site is further supported by the nonvariability of the absorption lines between the two epochs, which indicates a distance of the absorbing material of at least 560 pc from the burst.

The *Swift* satellite now provides faster information of the burst position and more early, high-resolution spectra can be obtained. Very early spectra, compared with later times, could also reveal possible changes of the absorption lines due to ionization of the ISM by the burst (Vreeswijk et al. 2007).

C. T. wants to thank Johan Fynbo, Alexander Kann, and Daniele Malesani for reading and improving the manuscript, useful discussions about technical issues and pointing out errors, and Alexander Kann in particular for providing the extinction law derived in his paper to flux-calibrate the spectra. Thanks also to Klaas Wiersema for the preprint of his paper on GRB 060218 and information about advanced line diagnostics. We would also like to thank the VLT staff for performing the target of opportunity UVES observations. The Dark Cosmology Centre is funded by the Danish National Research Foundation.

REFERENCES

Adelberger, K. L., Steidel, C. C., Shapley, A. E., & Pettini, M. 2003, ApJ, 584, 45
Asplund, M., Grevesse, N., Sauval, A. J., Allende Prieto, C., & Kiselman, D. 2004, A&A, 417, 751
Ballester, P., Dorigo, D., Disarò, A., Pizarro de La Iglesia, J. A., & Modigliani, A. 2000, in ASP Conf. Ser. 216, Astronomical Data Analysis Software and Systems IX, ed. N. Manset, C. Veillet, & D. Crabtree (San Francisco: ASP), 461
Barth, A. J., et al. 2003, ApJ, 584, L47
Berger, E., Penprase, B. E., Cenko, S. B., Kulkarni, S. R., Fox, D. B., Steidel, C. C., & Reddy, N. A. 2006, ApJ, 642, 979
Bloom, J. S., Berger, E., Kulkarni, S. R., Djorgovski, S. G., & Frail, D. A. 2003, AJ, 125, 999
Bond, N. A., Churchill, C. W., Charlton, J. C., & Vogt, S. S. 2001, ApJ, 557, 761
Bregman, J. 1980, ApJ, 236, 577
Bresolin, F., Garnett, D. R., & Kennicutt, R. C., Jr. 2004, ApJ, 615, 228
Butler, N., Ricker, G., Vanderspek, R., Ford, P., Crew, G., Lamb, D. Q., & Jernigan, J. G. 2005, ApJ, 627, L9
Cardelli, J. A., Clayton, G. C., & Mathis, J. S. 1989, ApJ, 345, 245
Castro, S., Galama, T. J., Harrison, F. A., Holtzman, J. A., Bloom, J. S., Djorgovski, S. G., & Kulkarni, S. R. 2003, ApJ, 586, 128
Chen, H. W., Prochaska, J. X., Bloom, J. S., & Thompson, I. B. 2005, ApJ, 634, L25
Christensen, L., Hjorth, J., & Gorosabel, J. 2004, A&A, 425, 913
Churchill, C. W., Kacprzak, G. G., & Steidel, C. C. 2005, in IAU Colloq. 199, Probing Galaxies through Quasar Absorption Lines, ed. P. R. Williams, C.-G. Shu, & B. Menard (Cambridge: Cambridge Univ. Press), 24
Churchill, C. W., Mellon, R. R., Charlton, J. C., Jannuzi, B. T., Kirhakos, S., Steidel, C. C., & Schneider, D. P. 2000, ApJ, 543, 577
Churchill, C. W., Vogt, S. S., & Charlton, J. C. 2003, AJ, 125, 98
Dekker, H., D'Odorico, S., Kaufer, A., Delabre, B., & Kotzlowski, H. 2000, Proc. SPIE, 4008, 534
D'Elia, V., et al. 2007, A&A, 467, 629
Dickey, J. M., & Lockman, F. J. 1990, ARA&A, 28, 215
Ellison, S. L., Mallén-Ornelas, G., & Sawicki, M. 2003, ApJ, 589, 709
Fiore, F., et al. 2005, ApJ, 624, 853
Fontana, E., & Ballester, P. 1995, ESO Messenger, 80, 37
Fox, A. J., Wakker, B. P., Savage, B. D., Tripp, T. M., Sembach, K. R., & Bland-Hawthorn, J. 2005, ApJ, 630, 332
Gehrels, N., et al. 2004, ApJ, 611, 1005
Gorosabel, J., et al. 2005, A&A, 444, 711
Greiner, J., Peimbert, M., Estaban, C., Kaufer, A., Jaunsen, A., Smoke, J., Klose, S., & Reimer, O. 2003a, GCN Circ. 2020, http://gcn.gsfc.nasa.gov/gcn3/2020.gcn3
Greiner, J., et al. 2003b, Nature, 426, 157
Hanuschik, R. W. 2003, A&A, 407, 1157
Heckman, T. M., Lehnert, M. D., Strickland, D. K., & Armus, L. 2000, ApJS, 129, 493
Hjorth, J., et al. 2003, Nature, 423, 847
Kann, D. A., Klose, S., & Zeh, A. 2006, ApJ, 641, 993
Kennicutt, R. C., Jr. 1998, ARA&A, 36, 189
Klose, S., et al. 2004, AJ, 128, 1942
Kobulnicky, H. A., Kennicutt, R. C., Jr., & Pizagno, J. L. 1999, ApJ, 514, 544
Kewley, L. J., Brown, W. R., Geller, M. J., Kenyon, S. J., & Kurtz, M. J. 2007, AJ, 133, 882
Kewley, L. J., & Dopita, M. A. 2002, ApJS, 142, 35
Ledoux, C., Vreeswijk, P., Smette, A., Jaunsen, A., & Kaufer, A. 2006, GCN Circ. 5237, http://gcn.gsfc.nasa.gov/gcn3/5237.gcn3
Lilly, S. J., Carollo, C. M., & Stockton, A. N. 2003, ApJ, 597, 730
Lipkin, Y. M., et al. 2004, ApJ, 606, 381
Masetti, N., et al. 2003, A&A, 404, 465
Matheson, T., et al. 2003, ApJ, 599, 394
Metzger, M. R., Djorgovski, S. G., & Kulkarni, S. R. 1997, Nature, 387, 878
Mirabal, N., et al. 2002, ApJ, 578, 818
Munari, U., & Zwitter, T. 1997, A&A, 318, 269
Osterbrock, D. E. 1989, Astrophysics of Gaseous Nebulae and Active Galactic Nuclei (Mill Valley, CA: Univ. Science Books)
Penprase, B. E., et al. 2006, ApJ, 646, 358
Perna, R., & Loeb, A. 1998, ApJ, 501, 467
Peterson, B. A., & Price, P. A. 2003, GCN Circ. 1985, http://gcn.gsfc.nasa.gov/gcn3/1985.gcn3
Piranomonte, S., D'Elia, V., Ward, P., Fiore, F., & Meurs, E. J. A. 2007, Proceedings of the Swift-Venice 2006 Meeting (astro-ph/0701563)
Prochaska, J. X., Chen, H.-W., & Bloom, J. S. 2006, ApJ, 648, 95
Prochaska, J. X., et al. 2007, ApJS, 168, 231
Rao, S. M., & Turnshek, D. A. 2000, ApJS, 130, 1
Reichart, D. E. 1998, ApJ, 495, L99
Savage, B. D., & Sembach, K. R. 1991, ApJ, 379, 245
Savaglio, S., & Fall, S. M. 2004, ApJ, 614, 293
Schlegel, D. J., Finkbeiner, D. P., & Davis, M. 1998, ApJ, 500, 525
Sollerman, J., Östlin, G., Fynbo, J. P. U., Hjorth, J., Fruchter, A., & Pedersen, K. 2005, NewA, 11, 103
Stanek, K. Z., et al. 2003, ApJ, 591, L17
Starling, R. L. C., Wijers, R. A. M. J., Hughes, M. A., Tanvir, N. R., Vreeswijk, P. M., Rol, E., & Salamanca, I. 2005, MNRAS, 360, 305
Tripp, T. M., & Bowen, D. V. 2005, in IAU Colloq. 199, Probing Galaxies through Quasar Absorption Lines, ed. P. R. Williams, C.-G. Shu, & B. Ménard (Cambridge: Cambridge Univ. Press), 5
Vanderspek, R., et al. 2003, GCN Circ. 1997, http://gcn.gsfc.nasa.gov/gcn3/1997.gcn3
van Paradijs, J., et al. 1997, Nature, 386, 686
Vreeswijk, P. M., et al. 2001, ApJ, 546, 672
———. 2007, A&A, 468, 83
Welty, D. E., Frisch, P. C., Sonneborn, G., & York, D. G. 1999, ApJ, 512, 636
Welty, D. E., Morton, D. C., & Hobbs, L. M. 1996, ApJS, 106, 533
Wiersema, K., et al. 2007, A&A, 464, 529
Williams, P. R., Shu, C.-G., & Ménard, B. 2005, IAU Colloq. 199, Probing Galaxies through Quasar Absorption Lines (Cambridge: Cambridge Univ. Press)